JET-P(95)25

Vapotron as Heat Sink for Flat High Conductivity Unidirectional CFC Tiles

H D Falter, D Ciric, A Celentano, C Ibbot, M Watson,
M Araki[1], S Suzuki[1], K Sato[1].

JET Joint Undertaking, Abingdon, Oxfordshire, OX14 3EA, UK.
[1] NBI Heating Laboratory, Naka Fusion Research Establishment, JAERI, 801-1 Naka-machi, Naka-gun, Ibaraki-ken, 311-01, Japan.

Preprint of a paper to be submitted for publication in
Fusion Technology

ABSTRACT

Two vapotrons from the JET actively cooled divertor design have been fitted by JAERI with unidirectional high conductivity CFC tiles and have been tested in the JET Neutral Beam Test Bed. The test section showed excellent uniformity and accepted power densities up to 30 MW/m^2 for equilibrium pulses. The surface temperature was 1100 °C at 20 MW/m^2. One tile detached at a power density of 25 MW/m^2. A total of just under 300 pulses at power densities mostly between 20 and 30 MW/m^2 have been fired onto the test sections without additional failure. The hydraulic parameters were: Water inlet temperature: 15 - 20 °C, average water pressure in the component: 0.4 and 0.69 Mpa, flow velocity: 6.9 and 7.5 m/s

1. INTRODUCTION

The actual power loading of the divertor plates in fusion experiments varies with confinement and stability of the plasma. Additionally the radiated fraction and the width and shape of the plasma footprint in the divertor region have a strong influence on the local power density, which is therefore not well known. At present all larger tokamak fusion experiments rely on the heat capacity of the armour tiles in the divertor region. Local melt damage is frequently observed. Future machines with longer pulse duration will have to use actively cooled target plates, consisting of an actively cooled heat sink and armour plates made from Carbon Fibre Composites (CFC), Beryllium, or refractory metals. These armour tiles have to tolerate transients with high power densities and the tile thickness must allow for erosion.

To assess the reliability and the limits of the present technology in brazing CFCs and Beryllium to Copper heat sinks, JET has previously tested several divertor mockups in collaboration with JAERI and NET [1]. This paper reports on the continuation of this program.

2. TEST SECTION

The test sections in this report have been manufactured jointly by JAERI and JET in the framework of a tripartite agreement between JAERI, JET, and TFTR. JET has supplied the heat sinks, JAERI the armour tiles. The heat sink is made from the partly finished vapotron elements as designed for the actively cooled JET divertor, made from CuCrZr and tapered in width from 36 mm at the wide end to 26 mm at the narrow end. The water channel is also tapered from 23 x 6.5 mm^2 at the narrow end to 30x4.5 mm^2 at the wide end (Fig.1).

One of these 816 mm long elements was cut into two halves and sent to JAERI for the brazing of the armour tiles made from unidirectional high conductivity Mitsubishi carbon fibre composites (MFC-1). The tile dimensions are 30 x 30 x 8 mm^3. The braze is an oven braze using TiCuSil.

Prior to brazing, machined MFC-1 tiles were outgassed in vacuum at a temperature of ~1000 °C to improve braze performance. Heat sink elements were then placed on top of the MFC-1 tiles arrayed in line with the TiCuSil braze filler metal foils. Temperature of the brazing components was increased to ~850 °C (in vacuum). After maintaining constant value for <5 minutes, temperature was gradually decreased to ambient temperature with a 10 °C/minute rate. Brazed MFC-1 tiles were slightly wider than the heat sink and the excessive material was cut off .

After brazing, the elements were neither quenched nor heat treated. The water feeds (at the top of Fig.2) were attached to the heat sink by e-beam welding after the brazing of the armour tiles. A photograph of the test sections before the test is shown in Fig.2.

3. TEST SET-UP

Fig.3 shows the assembly of the test sections. The test section is heated with a partially neutralised hydrogen ion beam with a typical acceleration voltage of 80 kV. Exposed is the top half of the test section over a height of 175 mm. The beam is scraped by two scrapers in the vertical direction. The test sections are clamped at the top and are free to move in the vertical plane at the bottom end. Both test sections are angled with nominally +5° and -5° respectively to the normal to protect the thermocouples connected to the inner sides of the vapotrons.

3.1 Instrumentation

3.1.1 Power:

The absorbed power in both test sections is measured by water calorimetry. Integration is performed over the water exit temperature measured outside the vacuum tank - approximately 2 m away from the test section. The water flow is measured individually with turbine flowmeters . One turbine flowmeter with a linear range of 10.2 - 159 m^3/h is in the common supply pipe to the test sections. Individual turbine flow meters are used to measure the return flow rate with a linear range of 1.4 - 13.6 m^3/h. The turbine flowmeters have been checked against each other by reducing the flow in one test section and comparing the reduction in the flow reading on the common flow meter at the inlet with that on the outlet.

3.1.2 Power density.

The peak power density is either derived from the absorbed energy and the vertical beam profile, or from the inertial calorimeter array installed 750 mm upstream of the test sections.

3.1.2.1 inertial calorimetry.

The inertial calorimeter array consists of individual cylindrical calorimeters with 10 mm diameter embedded in a cross shaped copper bar. The spacing of the calorimeters is 25 and

22.5 mm respectively in the vertical and horizontal plane. The power density on the inertial calorimeter has to be measured in short pulses. Errors can be made in the actual temperature reading, as there is not always a clear plateau in temperature after the pulse. Fig.4 shows the beam profiles from the inertial calorimeter. The temperature measurement is probably accurate to within 5% for the higher peaks and normally there is a visible cooldown, which makes the maximum temperature conservative. The peak power density from the inertial measurement is averaged over the width of one calorimeter block of 10 mm diameter.

3.1.2.2 water calorimetry

The peak power density from water calorimetry relies on the accuracy of flow, temperature and profile measurement. The vertical beam profile can be measured either with the inertial calorimeter array or it can be derived from the surface temperature profile of the test section. The e-folding length from the surface temperature is typically 10% less than that from the inertial profile. For simplicity an e-folding length of 105 mm is used for calculating the power density for all pulses. This e-folding length corresponds to that from the surface temperature profile. The horizontal beam profile is not folded into the calculation and the power density from water calorimetry is therefore averaged over the horizontal width of the test section.

3.1.2.3 comparison of the power densities

In a series of 92 consecutive pulses with fixed settings for the beam power, a scatter in power density from water calorimetry of approximately 5% is found. The power density derived from inertial calorimetry is 10% higher than the power density from water calorimetry on the right element, a measure of agreement which is regarded as tolerable.

The power density on the left element is measured to be 10% below that of the right element. This is most probably caused by a temperature drift in the water temperature signal leading to a faulty integral. It can be deduced from the surface temperature measurement and from the inertial beam profile that both test sections were exposed to the same power density.

To get a power density for each pulse an expression $p_d=a\times(P_{ex})^b$ is fitted with p_d as peak power density and P_{ex} as extracted beam power. A constant a of 19 and 17 is needed to fit the inertial and the calorimetric measurements. The exponent b is 1.2 in both cases, as observed previously. The fits are shown in Fig.5. Unless stated otherwise the extrapolated power density from the inertial measurement is used in this report.

3.2 Surface temperature

The surface temperature of the CFC is measured with an AGEMA THERMOVISION 900 imaging system with a frame rate of 15 Hz. The system is calibrated to within 1%. The highest calibrated temperature range is 500 - 2000°C for black body radiation. The test section is viewed from a distance of approximately 1.8 m and from an angle of roughly 30° to the

normal. Emissivity is set to match the surface temperature of the tile to the bulk temperature measured with thermocouples. The matching is done on the uncooled (dry) test sections during the radiative cooldown, when the gradients inside the test section can be neglected.

3.3 Flow velocity

When setting up the flow rates it was not realised that the water channel is tapered in width and height. A different flow rate in the two test sections was therefore used corresponding to the different average width of the water channel. The actual cross section of the water channel in the exposed area is however 140 mm^2 for both elements and the flow velocities are therefore 6.9 and 7.5 m/s for the flow rates of 3.5 and 3.8 m^3/h. Typical flow conditions valid for the test are listed in Table 1.

The water inlet temperature throughout the test was between 15 - 20 °C

Table 1: Flow conditions for the entire test - except the last two pulses

	average pressure (bar)	pressure drop (bar)	flow rate (m^3/h)
left test section	4	6.2	3.5
right test section	6.9	4.8	3.8

4. EXPERIMENTAL RESULTS

4.1 Test sequence

The test started up with the calibration of the IR imaging system. This was followed by approximately 25 clean up pulses at a power density of 10 MW/m^2. This set-up and clean up took approximately 100 seconds of exposure and was followed by a power scan starting from 5 MW/m^2 and increasing in steps of 5 MW/m^2. The test sequence is illustrated in Fig.6.

From the beginning the second tile from the top on the left element showed an overheating at the edge which appeared stable up to 15 MW/m^2. At 20 MW/m^2 the edge became hotter and at 25 MW/m^2 the tile detached essentially within one pulse. This is demonstrated in Fig.7 showing normalised horizontal profiles through the damaged tile and in Fig.8, where the development of the fault during the 25 MW/m^2 pulse is shown.

The detached tile was then removed from the test section and the remaining tiles where exposed to approximately 100 pulses at 20 MW/m^2. Finally the power density was increased up to 30 MW/m^2. The total exposure was just under 1500 s with approximately 300 cycles. All remaining tiles remained solidly attached to the heat sink.

The peak power density was limited by the critical heat flux in the heat sink, which was actually higher than in previous tests with similar vapotrons and flow velocities [2].

4.2 Surface temperature

Fig.9 shows a temperature contour plot taken at the end of a 20 MW/m^2 pulse (72472) before the detachment of the tile. The gaps between some of the tiles can be identified as localised hot spots. Apart from these hot spots a remarkably uniform temperature distribution is being observed. Only the edge of the second tile from the top on the left test section is clearly much hotter. To reduce the data the average temperatures in the areas AR01 and AR02 in Fig.9 are used to characterise the two test sections.

The time constant τ for the temperature rise is of the order of 0.8 seconds using an exponential law $T - T_0 = T_{eq} \times \left(1 - e^{-t/\tau}\right)$. This is shown in Fig.10 for a 20 and a 30 MW/m^2 pulse. At 30 MW/m^2 the time constant is slightly larger (0.9 s) and the temperature keeps rising slowly after the initial fast rise. The surface temperature as a function of time is shown in Fig.11 for 5 s pulses and all power densities. The pulses at low power density were done before the surface of the test sections was fully cleaned up and show a temperature step with beam on. This step has been observed before and is explained by loose particles on the surface [3].

The average surface temperature in the areas 01 and 02 is plotted against the power density from water calorimetry in Fig.12. On the right element the measured temperature agrees perfectly with the calculated temperature using the thermal conductivity of the armour tiles and the heat sink and a "global" heat transfer coefficient for the heat sink. This global heat transfer coefficient is derived from temperature measurements assuming one dimensional heat flow in the copper and a virtual flat exchange surface at the location of the fin root of the vapotron [4]. However to get a fit the heat transfer coefficient for a flow velocity of 11 m/s has to be used rather than that for the actual velocity of 7 m/s. The procedure of calculating the surface temperature is detailed in Annex 1.

On the left element the measured temperatures are slightly higher than those calculated assuming the same power density as on the right element. It is likely that this is caused by the lower flow velocity in the left element, and it will be shown below that the surface temperature is reduced when the flow velocity is increased.

4.2.1 Influence of flow velocity

In Fig.13 we show the horizontal profile of the surface temperature for two pulses with 25 MW/m^2. The water flow rate in the right element was constant at 3.8 m^3/h, that of the left element was varied between 3.5 and 4.5 m^3/h. With the higher flow velocity the temperature drops by approximately 100 °C. An interesting structure in the surface temperature is observed: The temperature is high at the edges and in the centre, as if the test section had two cooling

channels on either side of the centre line. This increased cooling could be explained by the geometrical restriction of the water inlet geometry, which forces the flow sideways - similar to a thumb on a water tap. A corresponding flow distribution has also been observed in a test developed to measure the thermal integrity of similar composite armour plates [5]. In this test the component is covered with frost and the defrosting sequence is observed when the heat sink is heated up by water flowing through the cooling channel (Fig.14).

5. DISCUSSION

5.1 Power density.

The power density from water calorimetry measured on the left element appears to be too low. The beam was well centred and the power densities on both elements must have been almost identical. This is confirmed by the surface temperature which was almost the same on both elements.

The discrepancy between the inertial measurement and water calorimetry is a frequently observed phenomenon. One obvious reason is that the integration over the water temperature signal misses some energy which is left in the component and connecting pipework at the end of the integration. The actual discrepancy of 10 % can be regarded as quite good agreement particularly as the water calorimetry averages over the width of the test section.

The peak power density of 30 MW/m^2 achieved in these tests is the highest reported as being successfully withstood by a brazed CFC joint. Power densities above 20 MW/m^2 have only been achieved previously with the externally finned swirl tube design pioneered by JAERI [6]. This high power density and the excellent uniformity of the surface temperature show that the brazing technique used is almost perfect.

The monoblock design, which was almost unbreakable in tests [7,8], might have a similar strength, but the very high surface temperatures observed on some of the tiles prevented this from being verified.

5.2 Mechanical integrity

Taking into account that this is a new development of brazing unidirectional CFCs to CuCrZr, the quality of the joints is excellent with only one failure. However the failure shows that faults tend to grow quickly in this design, leading to a rapid and complete detachment of the tile. Further improvements could be achieved by optimising the edge geometry at the transition from armour to heat sink. The failure mode might be improved by interlocking armour and heat sink. However this would have a negative effect on the option of in situ repairs.

5.3 Critical heat flux and pressure drop

Even at the highest power density (28 - 32 MW/m^2) there was no sign of a critical heat flux. This is surprising at a flow rate of 7 m/s. Similarly the surface temperature suggests a better cooling than expected at 7 m/s. The reason for this could be the additional turbulence created by the restricted inlet geometry. The pressure drop in these elements is higher than expected from similar narrow vapotrons tested previously (see ref. 2). The high heat flux the tiles except, the increased pressure drop and the structure on the surface temperature profile all indicate a locally increased flow velocity.

REFERENCES

[1] H D Falter, D Ciric, E B Deksnis, P Massmann, K N Mellon, A Peacock, M Araki, K Sato, S Suzuki, A Cardella, "Comparison between actively cooled Divertor dump plates with beryllium and CFC armour", Fusion Technology 94, Proceedings of the 18th Symposium on Fusion Technology (SOFT), held in Karlsruhe, Germany, 22-26 August 1994, ISBN: 0 444 82220 8 and JET-P(94)40

[2] H D Falter, E Thompson, "Performance of hypervapotron beam stopping elements in JET". Fusion Technology this issue

[3] D Ciric et al, "Light Emission from Graphite Surfaces during beam bombardment, Observation and Consequences for use of Graphite in Divertors". Fusion Technology 94, Proceedings of the 18th Symposium on Fusion Technology (SOFT), held in Karlsruhe, Germany, 22-26 August 1994, ISBN: 0 444 82220 8 and JET-P(94)40, page19

[4] H D Falter et al., "Thermal test results of the JET divertor plates", High Heat Flux Engineering, Ali M. Khousanory, Editor, Proc. SPIE 1739, p 162 (1992)

[5] H D Falter, D Ciric, F D Long, "Visualisation of thermal contact with a commercial CCD video system", Fusion Technology 94, Proceedings of the 18th Symposium on Fusion Technology (SOFT), held in Karlsruhe, Germany, 22-26 August 1994, ISBN: 0 444 82220 8 .

[6] S Suzuki, M Akiba, M Araki, K Satoh, K Yokoyama, M Dairaku, "High heat flux experiments of saddle type divertor module", Journal of Nuclear Materials 212-215 (1994) 1365-1369

[7] M Araki, S Suzuki, M Akiba, M Dairaku, R Duwe, J Linke, E. Wallure, K Yokoyama, I Smid, M Ogawa, S Tanaka, Y Ohara, K Nakamura, "Development and Testing of divertor Mock-ups for ITER/FER at JAERI", Proceedings of the 17th Symposium on Fusion Technology, Rome, Italy, 14 - 18 Sept. 1992, ISBN: 0 444 89995 2

[8] A Cardella, G P Celata, G Dell'Orco, G P Gaspari, G Cattadori, A Mariani, "Thermal hydraulic Experiments for the NET divertor" , Proceedings of the 17th Symposium on Fusion Technology, Rome, Italy, 14 - 18 Sept. 1992, ISBN: 0 444 89995 2.

ANNEX 1: ONE DIMENSIONAL CALCULATION OF THE SURFACE TEMPERATURE.

At the location of the fin root, 3 mm below the surface of the vapotron, we assume a heat exchange surface with a global heat transfer coefficient h_{global} The temperature drop across this surface is then

$$\Delta T_{ex} = p \div h_{global} \tag{1}$$

with p as power density. In the copper we assume a constant thermal conductivity k_{CuCrZr} and the gradient is

$$(dT/dZ)_{copper} = p \div k_{CuCrZr} \tag{2}$$

For the CFC tile we fit the measured thermal conductivity by the expression

$$k_{CFC}(T) = -111.1\left[\frac{W}{m \times K}\right]\ln(T/8851) \tag{3}$$

with T being the temperature in °C. The gradient through the CFC is then

$$(dT/dZ)_{CFC} = p \div k_{CFC}(T) \tag{4}$$

The boundary condition for the numerical solution is the bulk water temperature, taken as 0 °C for simplicity. Fig.15 shows the result. We see that the actual thermal conductivity of the CuCrZr is of minor importance. The calculated surface temperatures can be fitted with the expression

$$T(p) = \alpha \times p^{1.2}$$

where T is in °C, p is in W/m^2, and $\alpha = 1.9 \times 10^{-6}$ for h_{global} = 70 000$W/m^2/K$.

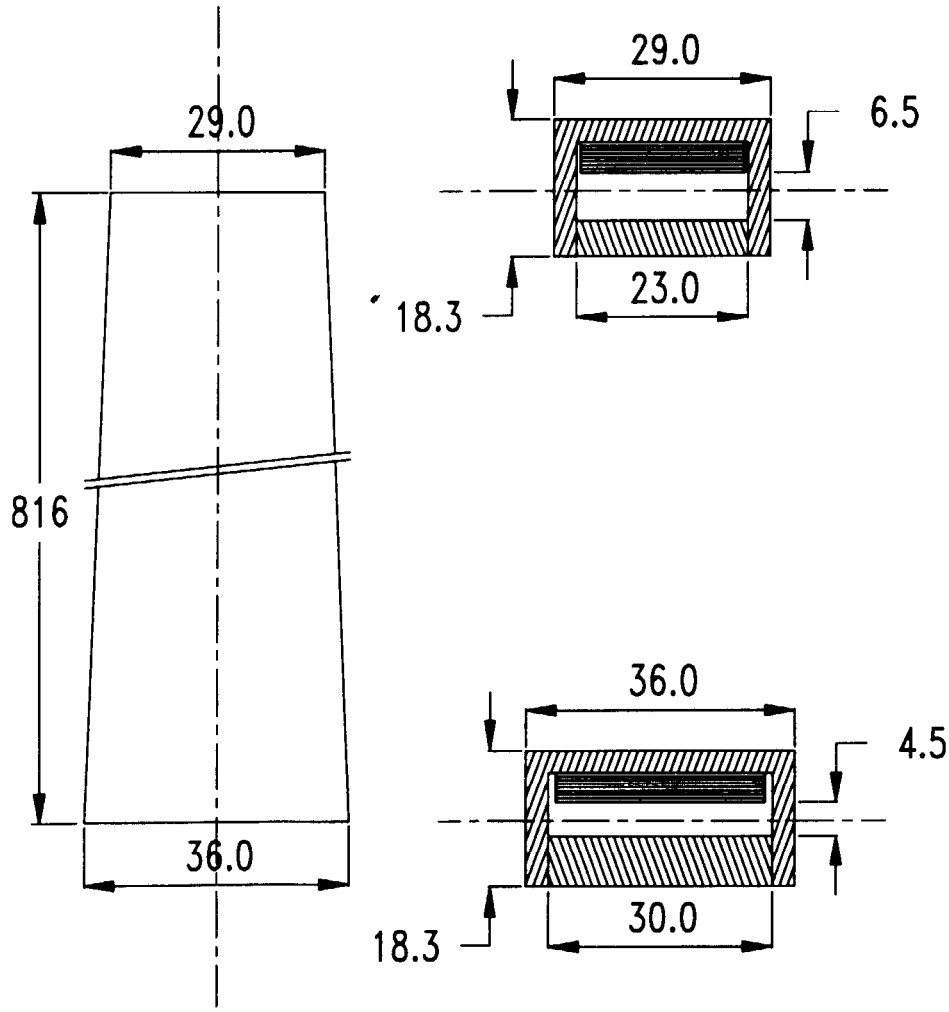

Fig.1: Dimensions of the vapotron used as heat sink. The water channel is tapered from 30x4.5 mm^2 to 23x6.5 mm^2.

Fig.2: Photograph of the test assembly. The support and the water feed is at the top of the test sections.

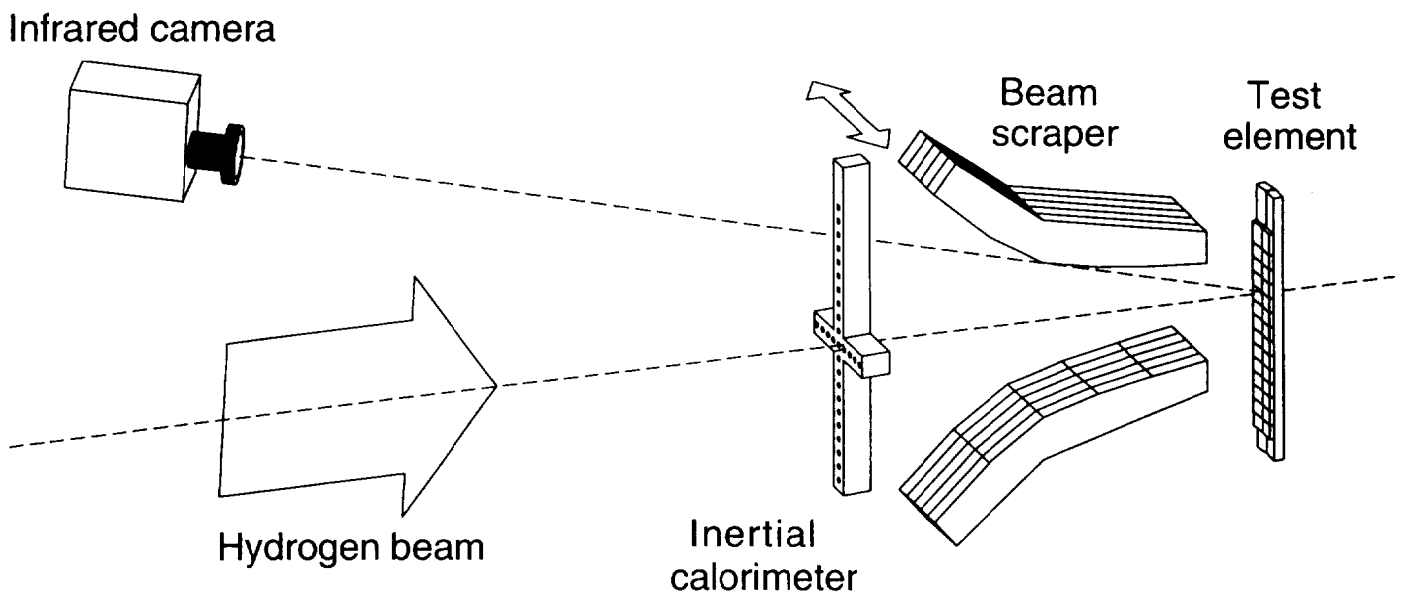

Fig.3: Schematic of the test set-up.

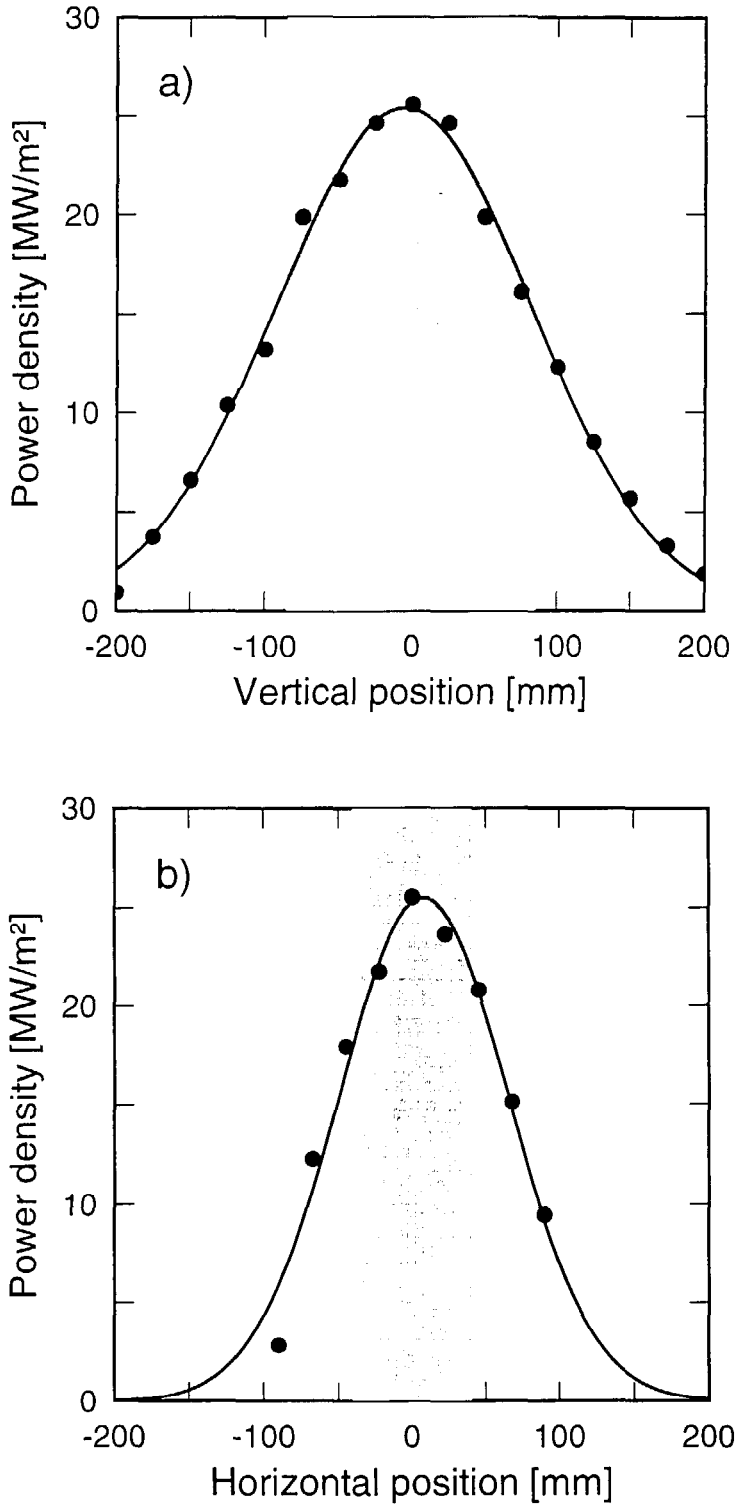

Fig.4: Beam profiles from the inertial diagnostic. The location of the test sections is shown as grey area. Power density varies over the width by 30%.

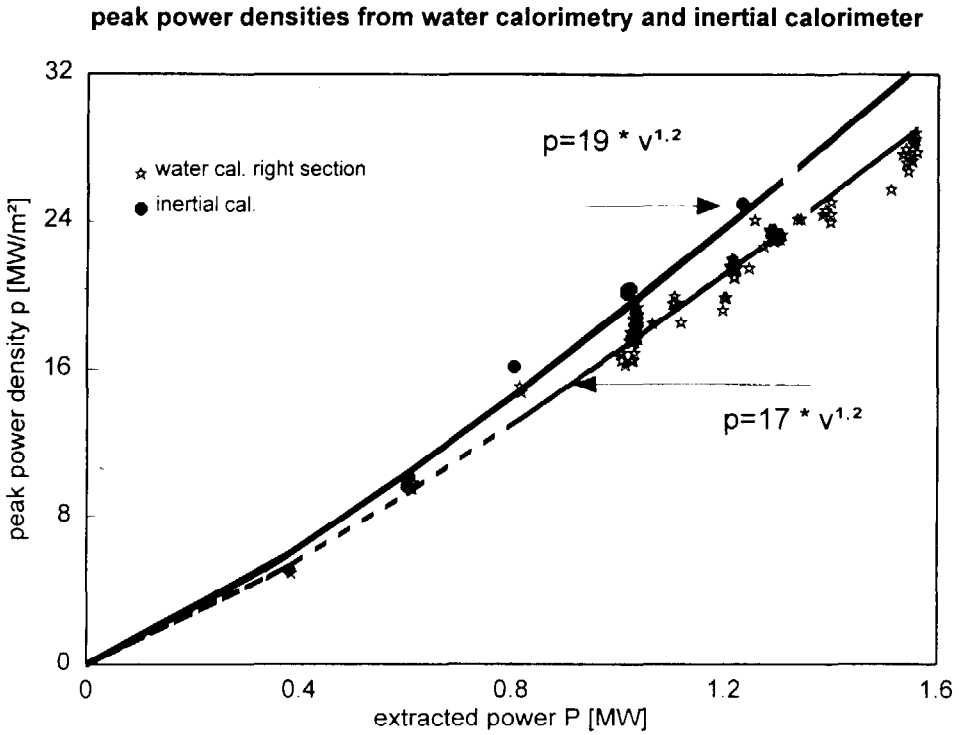

Fig.5: Inertial and calorimetric peak power density as a function of the extracted power. The scatter is approximately 5%. The difference between inertial measurement and water calorimetry is 10%.

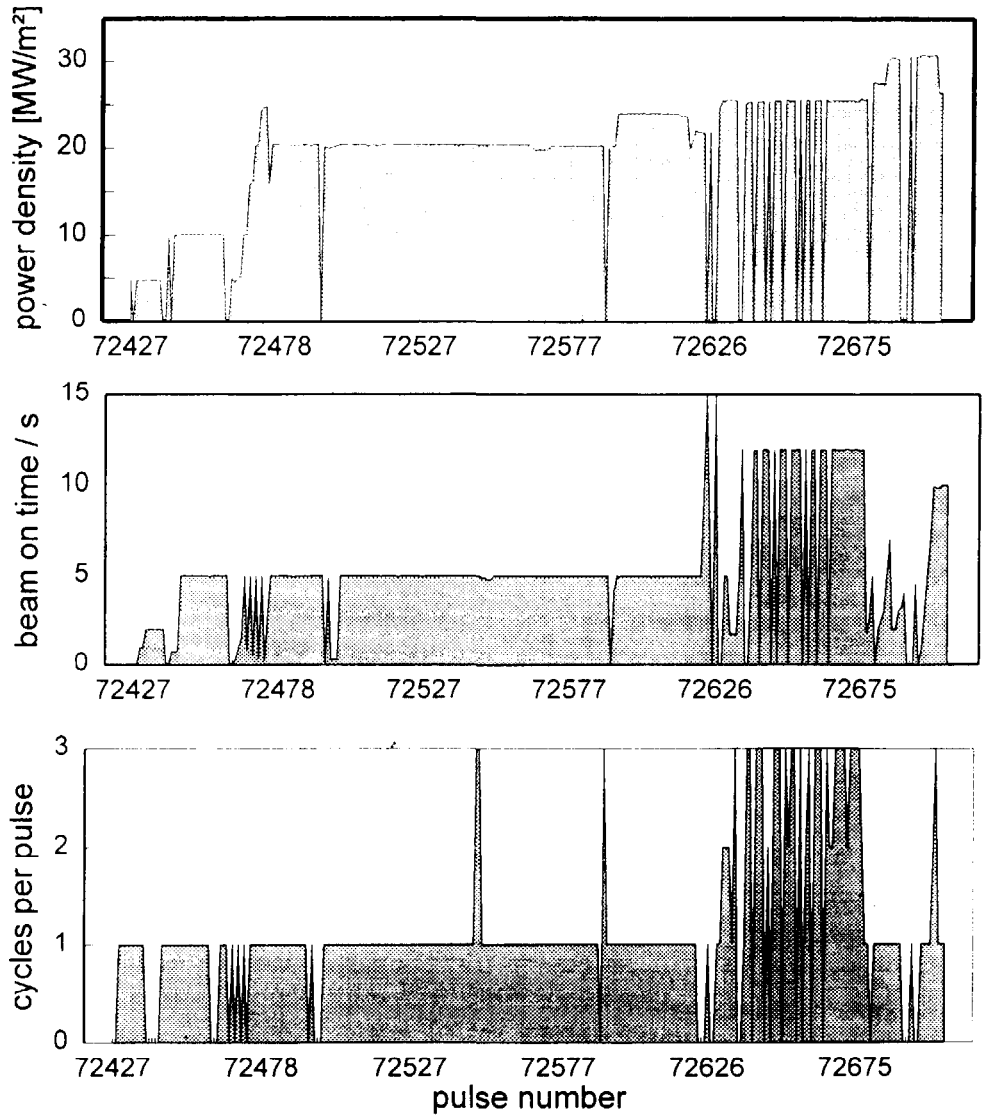

Fig.6: Test sequence with peak power density (top), beam on time (middle) and cycles per pulse (bottom) for all pulses.

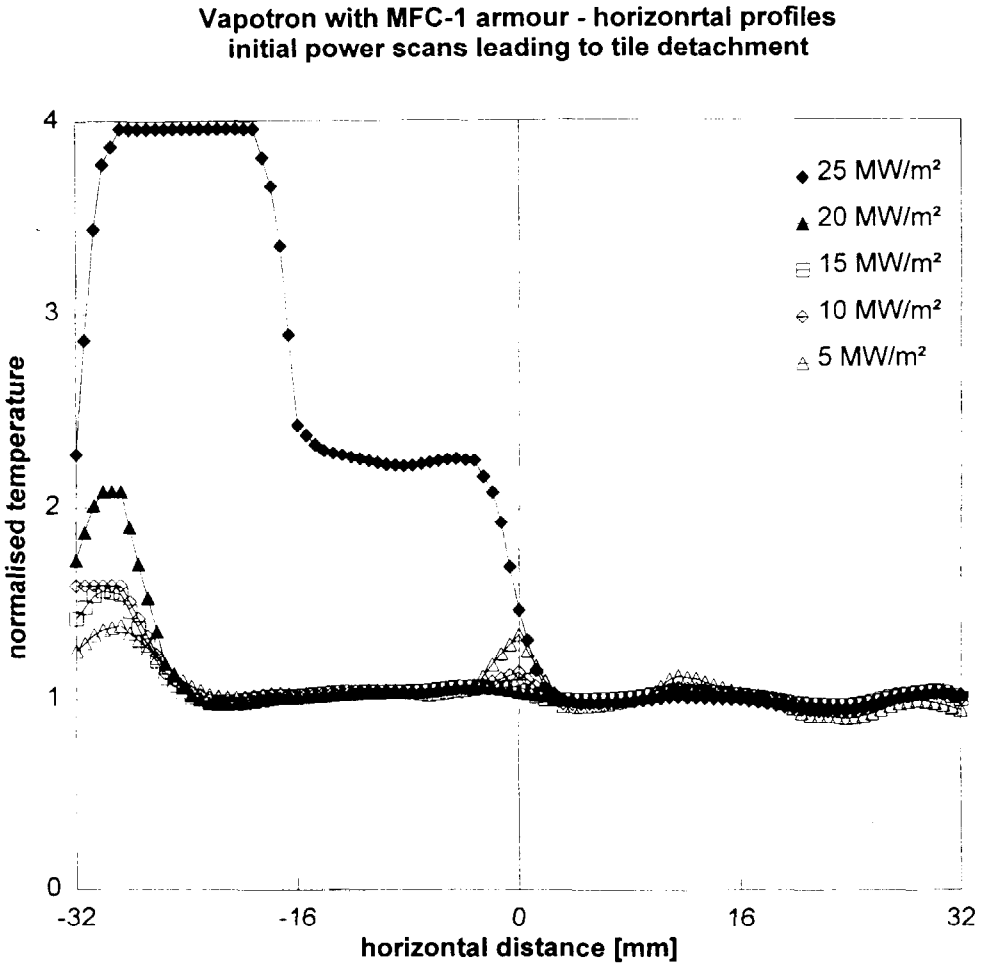

Fig.7: Normalised horizontal beam profile through both test sections. Initially the temperatures at both test sections are almost identical. The left edge is always overheated. At 25 MW/m^2 the left tile lost contact.

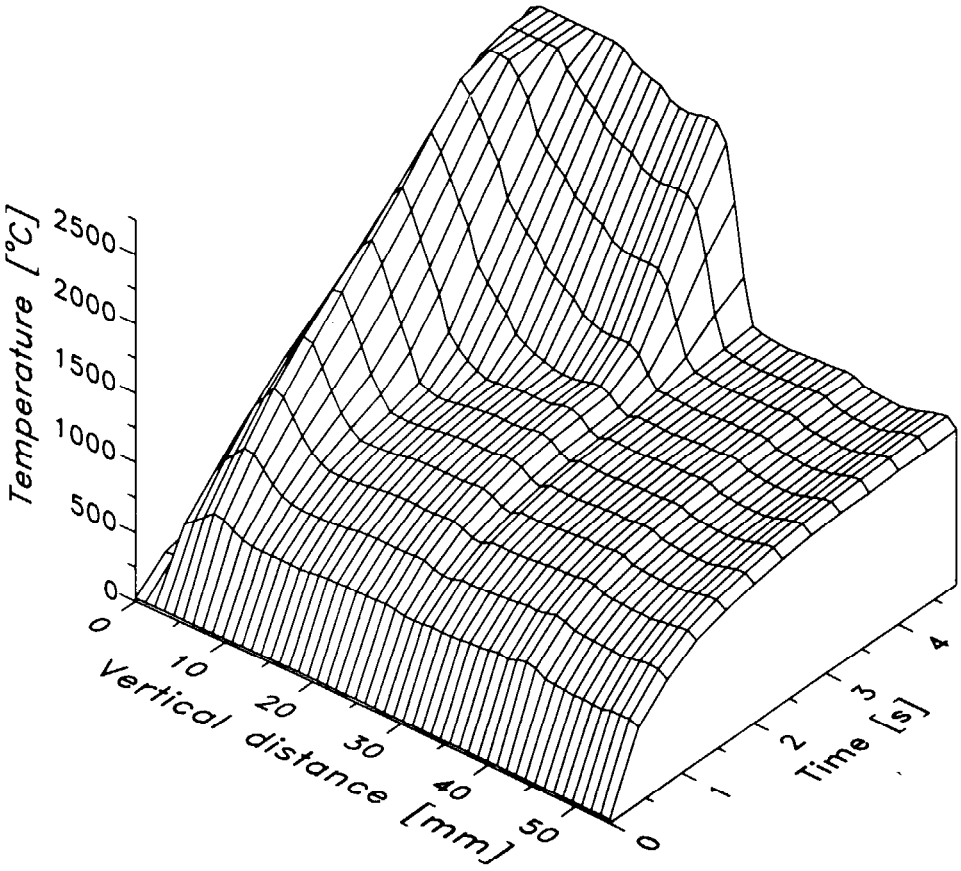

Fig.8: Horizontal profiles as in Fig. 7 showing the gradual detachment of the tile within one pulse.

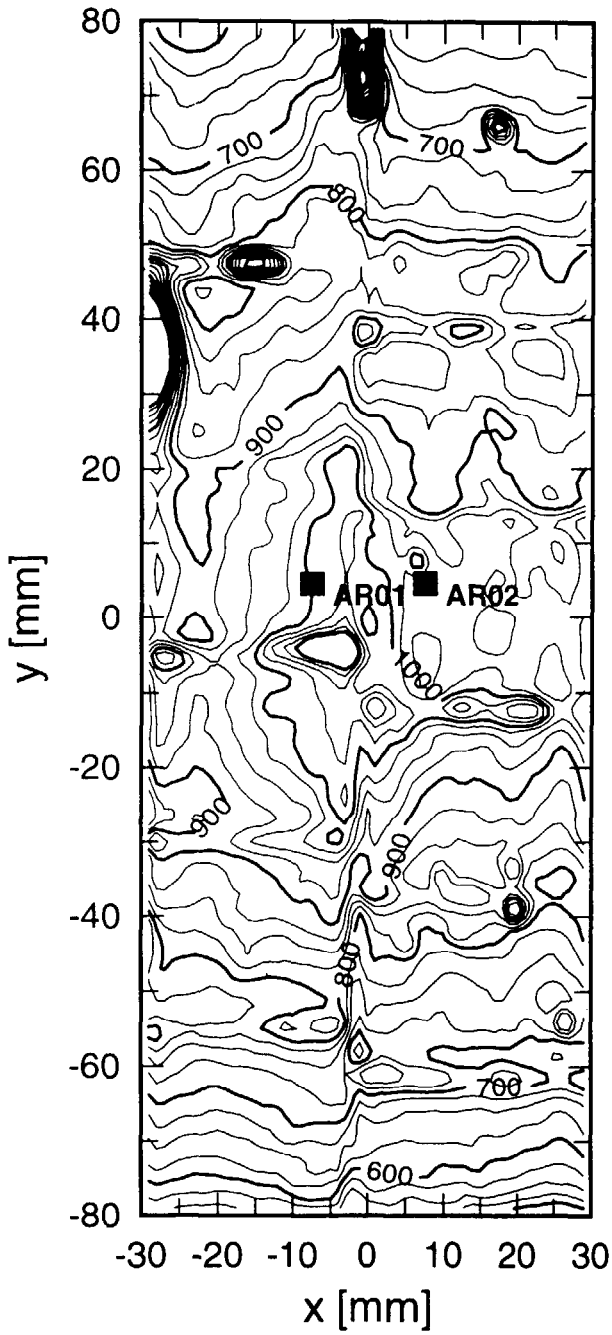

Fig.9: Contour plot of the surface temperature distribution at 20 MW/m^2. The areas AR01 and AR02 are marked. The average temperature in these areas is used to characterise the two test sections.

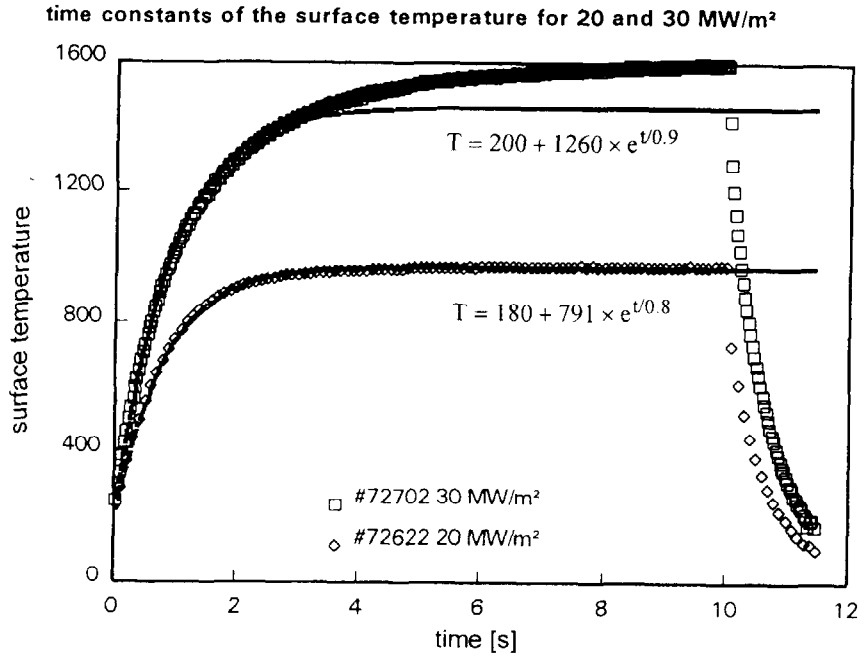

Fig.10: Time constants of the surface temperature at 20 and 30 MW/m^2. At the lower power density the temperature follows the exponential fit and reaches equilibrium after 4 seconds. At the higher temperature the temperature shows a slight rise up to 10 seconds.

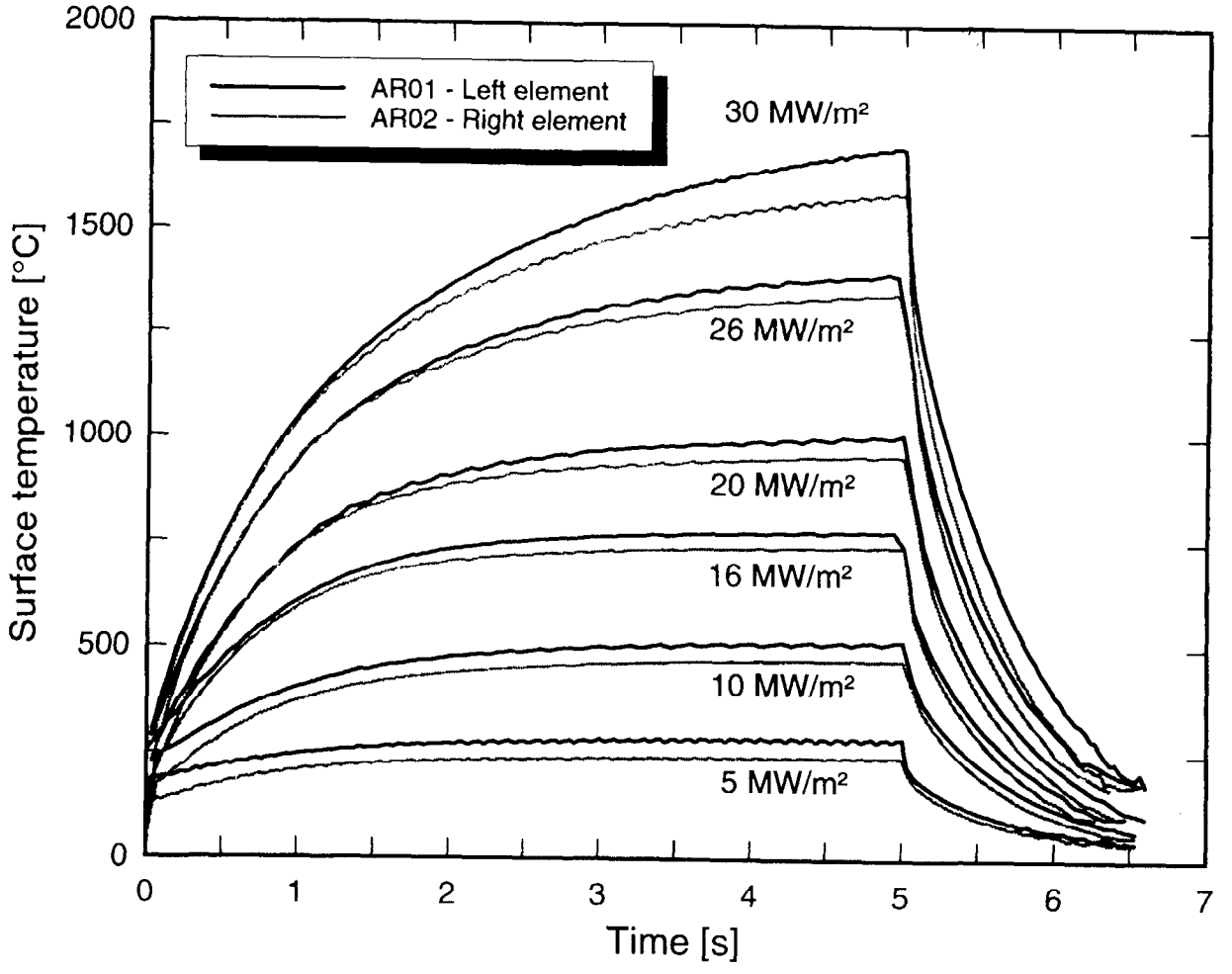

Fig.11: Surface temperature as a function of time in 5 second pulses for all power densities. With increasing power density it takes longer for the surface to reach equilibrium.

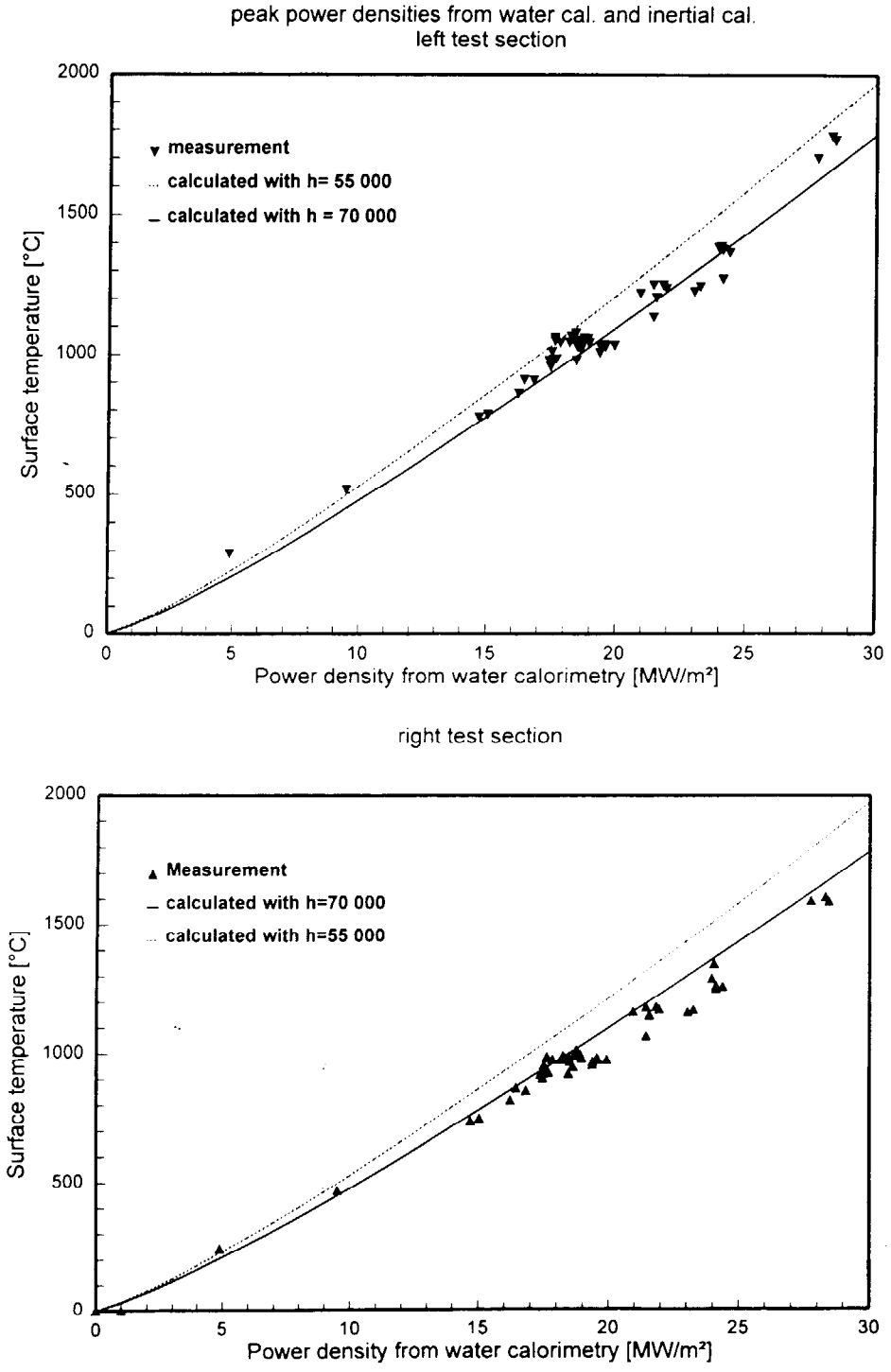

Fig.12: Surface temperature plotted against power density from water calorimetry. The temperatures agree perfectly with the calculated temperatures for the right element. The left element shows slightly higher temperatures due to lower flow velocity.

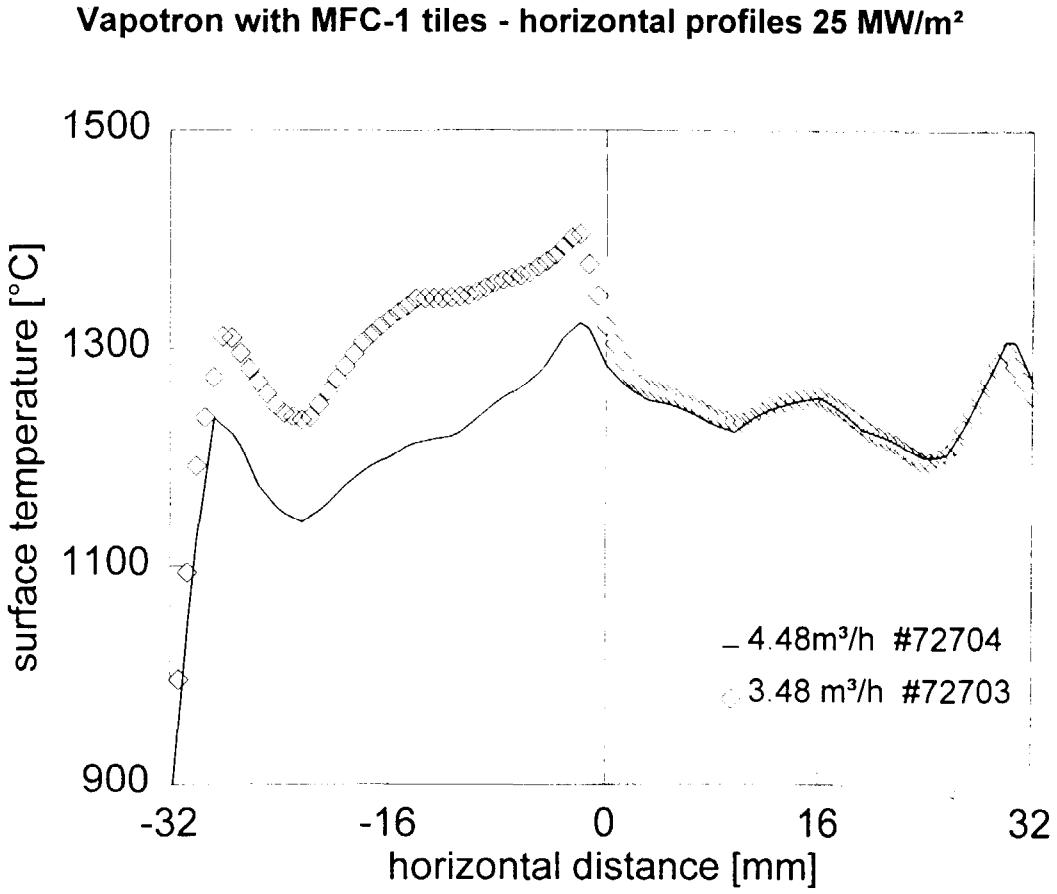

Fig.13: Horizontal surface temperature profile for two different flow rates in the left element. At the higher flow velocity the temperature of the left test section is reduced by approximately 100 °C. Minima in surface temperature are observed on either side of the centre line of each test section.

Fig.14: Defrosting of the precooled test section with water in the cooling channel. Top: panel installed horizontally. Gravity increases the flow velocity and the heat transfer at the bottom. Below: Three time slices of the vertical test section. Defrosting starts at either side of the centre line indicating a better heat transfer at this location.

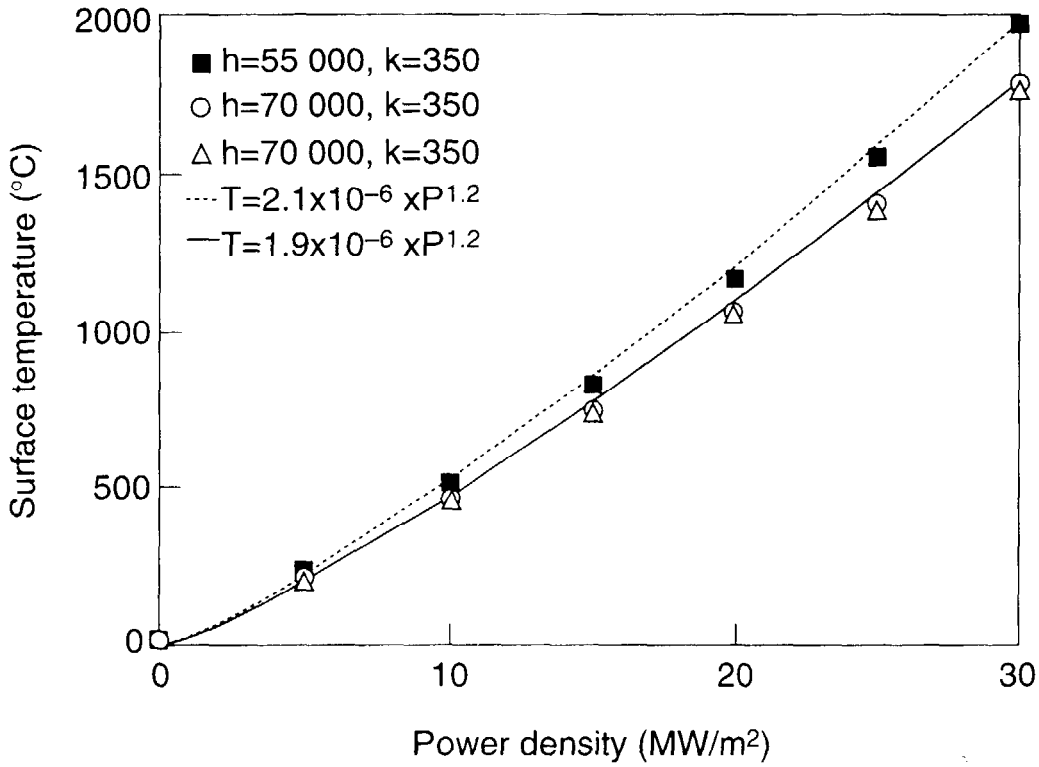

Fig.15: Calculated surface temperature using 55 000 and 70 000 W/m^2/K as global heat transfer coefficient and 350 and 370 W/m/K as thermal conductivity of the CuCrZr heat sink. The thermal conductivity of the MFC-1 was taken as .

$$K_{CfC} = -111.1\ \ell n \frac{T}{8851} \quad \frac{W}{mK}$$